PHYSICAL REVIEW B **87**, 115115 (2013)

Hybrid NRG-DMRG approach to real-time dynamics of quantum impurity systems

Fabian Güttge,[1] Frithjof B. Anders,[1] Ulrich Schollwöck,[2] Eitan Eidelstein,[3,4] and Avraham Schiller[3]
[1]*Lehrstuhl für Theoretische Physik II, Technische Universität Dortmund, 44221 Dortmund, Germany*
[2]*Physics Department, Arnold Sommerfeld Center for Theoretical Physics, and Center for NanoScience, Ludwig-Maximilians-Universität München, D-80333 München, Germany*
[3]*Racah Institute of Physics, The Hebrew University, Jerusalem 91904, Israel*
[4]*Department of Physics, NRCN, P.O. Box 9001, Beer-Sheva 84190, Israel*
(Received 8 June 2012; published 11 March 2013)

A hybrid approach to nonequilibrium dynamics of quantum impurity systems is presented. The numerical renormalization group serves as a means to generate a suitable low-energy Hamiltonian, allowing for an accurate evaluation of the real-time dynamics of the problem up to exponentially long times using primarily the time-adaptive density-matrix renormalization group. In particular, by constructing a suitable hybrid chain, discretization errors are essentially eliminated on all time scales of interest. We extract the decay time of the interaction-enhanced oscillations in the interacting resonant-level model and show their quadratic divergence with the interaction strength U. Our numerical analysis is in excellent agreement with analytic predictions based on an expansion in $1/U$.

DOI: 10.1103/PhysRevB.87.115115 PACS number(s): 73.21.La, 73.63.Rt, 72.15.Qm

I. INTRODUCTION

The description of strong electronic correlations far from thermal equilibrium poses an enormous theoretical challenge. At the root of the problem lies the nonequilibrium density operator, which is not explicitly known in the presence of interactions. Of particular relevance are quench and driven dynamics realized in pump-probe experiments,[1,2] atomic traps,[3,4] and nanodevices,[5,6] where the full-time evolution of the density operator should, in principle, be tracked.

Quantum impurity systems (QIS's) have regained considerable attention over the past 15 years due to the advent of carefully designed nanodevices. These generically consist of a few locally interacting degrees of freedom, typically a quantum dot, in contact with macroscopic leads. Since driven dynamics in nanodevices is of practical relevance to quantum computing and quantum control, considerable efforts were mounted in recent years toward devising approaches capable of treating the nonequilibrium state in QIS's. Indeed, significant analytical progress was achieved in the calculation of real-time dynamics using different adaptations of perturbative renormalization-group ideas.[7–10] However, with the exception of Ref. 11, these approaches are confined to the weak-coupling regime. Numerical methods, such as applications of the time-dependent density-matrix renormalization group (TD-DMRG)[12,13] to QIS's,[14,15] the time-dependent numerical renormalization group (TD-NRG),[16,17] an iterated path-integral approach,[18] and different continuous-time Monte Carlo simulations,[19–21] are more flexible in the parameter regimes they can treat, but are either restricted to short time scales[14,15,18–21] or susceptible to finite-size and discretization errors.[14–17] Indeed, finite-size representations are faced with an inherent difficulty of accurately representing the continuum limit even on intermediate time scales.

In this paper, we report the extension of a recent hybrid approach[22] that overcomes some of the major obstacles hampering the description of quench dynamics in QIS's. The basic idea is to exploit the outstanding capabilities of the TD-NRG to bridge vastly different time scales in order to systematically construct an effective low-energy Hamiltonian, whose real-time dynamics can be calculated using complementary approaches that do not rely on the special structure of the Wilson chain. In this manner, one can largely eliminate discretization errors inherent to the Wilson chain while boosting the complementary approach to time scales orders of magnitude beyond its natural capabilities. As a proof of principle, we have hybridized in Ref. 22 the TD-NRG with the Chebyshev expansion technique (CET),[23] yet the limited Hilbert space accessible to the CET restricted us to the standard Wilson chain.

Here, we demonstrate the full power of the approach by hybridizing the TD-NRG with the TD-DMRG,[13] which allows us to lift the restriction to an ordinary Wilson chain. Using the exactly solvable noninteracting resonant-level model as a benchmark, we discuss the role of different chain types in faithfully reproducing the real-time dynamics of the original continuum model, proposing a new chain structure that circumvents the main drawback of the Wilson chain used in the TD-NRG and also in Ref. 22. From the standpoint of the TD-DMRG, our approach enables access for the first time to exponentially long time scales in units of the inverse bandwidth.

Focusing on the interacting resonant-level model (IRLM),[24,25] we show that one can essentially eliminate discretization errors on all time scales of interest by constructing a suitable hybrid chain. This, in turn, allows for a thorough examination of the interaction-enhanced oscillations first reported in Ref. 22, yielding excellent agreement with analytical predictions for their frequency and damping time. The latter is shown to diverge quadratically with the interaction strength, demonstrating that relaxation to equilibrium can involve new time scales far longer than the thermodynamic ones.

The remainder of the paper is organized as follows. In Sec. II we present the hybrid NRG-DMRG approach, starting with a concise derivation of the hybrid-NRG platform in Sec. II A, followed by details of the NRG-DMRG interface in Sec. II B. Our results are presented in turn in Sec. III. To this end, we begin with a brief exposition of the IRLM in Sec. III A, followed by the introduction of the double Wilson chain in Sec. III B and a comprehensive analysis of

the interaction-enhanced oscillations in Sec. III C. Details of the strong-coupling expansion are relegated to an Appendix. We conclude in Sec. IV with a brief summary and outlook.

II. HYBRID NRG-DMRG

A. Concise derivation of the hybrid-NRG

The hybrid-NRG platform was thoroughly discussed in Ref. 22 from a wave-function perspective. Below we present an alternative derivation of the platform based on the TD-NRG. The Hamiltonian $\mathcal{H} = \mathcal{H}_{\rm bath} + \mathcal{H}_{\rm imp} + \mathcal{H}_{\rm mix}$ of a quantum impurity problem consists of three parts: $\mathcal{H}_{\rm bath}$ models the continuous bath, $\mathcal{H}_{\rm imp}$ represents the decoupled impurity, and $\mathcal{H}_{\rm mix}$ describes the coupling between the two subsystems. For $t < 0$, the entire system is assumed to be characterized by a density operator $\hat{\rho}_0$ associated with an initial Hamiltonian $\mathcal{H}^i$. Specifically, $\hat{\rho}_0$ can either be the equilibrium density operator corresponding to $\mathcal{H}^i$, or may project onto one of its low-lying eigenstates, typically the ground state. At time $t = 0$, a static perturbation is abruptly switched on such that $\mathcal{H}^i \to \mathcal{H}^f$. Our goal is to track the time evolution of local expectation values: $O(t) = {\rm Tr}\{\hat{\rho}(t)\hat{O}\}$ with $\hat{\rho}(t) = e^{-it\mathcal{H}^f}\hat{\rho}_0 e^{it\mathcal{H}^f}$.

In Wilson's numerical renormalization group (NRG),[26] $\mathcal{H}_{\rm bath}$ is discretized logarithmically using a dimensionless parameter $\Lambda > 1$, and mapped onto a semi-infinite chain whose open end is coupled to the impurity via $\mathcal{H}_{\rm mix}$. Wilson's chain is characterized by exponentially decreasing hopping matrix elements $t_m \propto D\Lambda^{-m/2}$ (D being the conduction-electron bandwidth), defining a natural separation of scales. This enables an iterative diagonalization of $\mathcal{H}$, where at the conclusion of each step only the lowest N_s eigenstates of that iteration are retained. Terminating the procedure after N steps, the collection of states discarded after each iteration combine to form a complete basis set of approximate NRG eigenstates of $\mathcal{H}$ on the N-site chain.[16,17] The expectation value of any local operator $\hat{O}$ can be formally expressed as[16,17]

$$O(t \geqslant 0) = \sum_{m=0}^{N} \sum_{r,s}^{\rm trun} O^m_{r,s}\rho^m_{s,r}(t), \tag{1}$$

where r and s run over the NRG eigenstates of $\mathcal{H}^f$ at iteration $m \leqslant N$, $O^m_{r,s}$ is the matrix representation of $\hat{O}$ at that iteration, and $\rho^m_{s,r}(t)$ is the corresponding time-dependent reduced density matrix. The restricted sum over r and s requires that at least one of these states is discarded at iteration m.

Partitioning the sum over m into $m \leqslant M$ and $M < m$ at some arbitrary but fixed $M < N$, Eq. (1) is recast as

$$O(t \geqslant 0) = \sum_{m=0}^{M} \sum_{r,s}^{\rm trun} O^m_{r,s}\rho^m_{s,r}(t) + {\rm Tr}\{\hat{1}^+_M \hat{O} \hat{1}^+_M \hat{\rho}(t) \hat{1}^+_M\}, \tag{2}$$

where $\hat{1}^+_M$ projects onto the subspace retained at the conclusion of iteration M. Equation (2) is formally exact, relying solely on the completeness of our basis set.[16,17] It has the following interpretation. At each energy scale $D\Lambda^{-m/2}$ with $m \leqslant M$, only those terms involving at least one discarded high-energy state contribute to $O(t)$, leaving the contribution of the low-energy subspace retained at the conclusion of iteration M. In the process, the NRG has produced an effective quantum-impurity Hamiltonian $\mathcal{H}_{M+1}$ with the reduced bandwidth $D_{\rm eff} \propto D\Lambda^{-M/2}$:

$$\mathcal{H}_{M+1} = \sum_k E^M_k |k;M\rangle\langle k;M| + \sum_{m=M}^{N-1} \sum_\nu t_m \hat{1}^+_M \{f^\dagger_{m+1,\nu} f_{m,\nu} + {\rm H.c.}\} \hat{1}^+_M. \tag{3}$$

Here, $f^\dagger_{m,\nu}$ creates an electron of flavor (spin) ν on the chain site m, $|k;M\rangle$ labels the kept NRG eigenstates at iteration M, and E^M_k are the corresponding NRG eigenenergies. Usually, one would proceed with the NRG to iteratively diagonalize $\mathcal{H}_{M+1}$. Here, we follow a different route: (i) we abandon the traditional Wilson chain and seek an optimal choice for the hopping amplitudes t_m with $m \geqslant M$; (ii) $\mathcal{H}_{M+1}$ is used as input for our complementary method of choice in order to compute ${\rm Tr}\{\hat{1}^+_M \hat{O} \hat{1}^+_M \hat{\rho}(t) \hat{1}^+_M\}$; (iii) employing the standard NRG approximation[16,17] $\rho^m_{s,r}(t) \approx e^{i(E^m_r - E^m_s)t}\rho^{\rm red}_{s,r}(m)$, the reduced density matrix $\rho^{\rm red}_{s,r}(M)$ as produced by our method of choice is fed back into the TD-NRG to account for the remaining high-energy dynamics in Eq. (2).

In this paper, we supplement the TD-NRG with the adaptive TD-DMRG.[13] The system is assumed to initially occupy the ground state $|\psi_0\rangle$ of $\mathcal{H}^i_{M+1}$, which we construct using the DMRG.[27] Accordingly, the time-dependent density operator $\hat{\rho}(t)$ is given by

$$\hat{\rho}(t) = |\psi(t)\rangle\langle\psi(t)| \tag{4}$$

with

$$|\psi(t)\rangle = e^{-it\mathcal{H}^f}|\psi_0\rangle, \tag{5}$$

resulting in

$${\rm Tr}\{\hat{1}^+_M \hat{O} \hat{1}^+_M \hat{\rho}(t) \hat{1}^+_M\} = \langle\chi_M(t)|\hat{O}|\chi_M(t)\rangle. \tag{6}$$

Here, $|\chi_M(t)\rangle = \hat{1}^+_M|\psi(t)\rangle$ is the projection of $|\psi(t)\rangle$ onto the low-energy subspace retained at the conclusion of iteration M of the final Hamiltonian $\mathcal{H}^f$.

Although Eq. (2) is formally exact for arbitrary M, the larger $N_\chi = \langle\chi_M(t)|\chi_M(t)\rangle \leqslant 1$, the smaller the contribution of the sum on the right-hand side of Eq. (2). If $(1 - N_\chi) < \epsilon$ for some small number ϵ, then $|\chi_M(t)\rangle = |\psi(t)\rangle + \mathcal{O}(\sqrt{\epsilon})$, and the major contribution to the real-time dynamics originates from $\langle\chi_M(t)|\hat{O}|\chi_M(t)\rangle$.

A proper choice of M is therefore important. Initially, the NRG level flows[26] of $\mathcal{H}^i$ and $\mathcal{H}^f$ are nearly identical. We choose M to be a characteristic iteration after which the two level flows begin to significantly deviate from one another.[16,17,26] The corresponding energy scale, $D\Lambda^{-M/2}$, is typically of order the energy difference between $\langle\psi_0|\mathcal{H}^i|\psi_0\rangle$ and $\langle\psi_0|\mathcal{H}^f|\psi_0\rangle$. With that choice of M, the major contribution to $O(t)$ stems from $\langle\chi_M(t)|\hat{O}|\chi_M(t)\rangle$. We approximate $|\chi_M(t)\rangle$ by $\exp(-it\mathcal{H}^f_{M+1})\hat{1}^+_M|\psi_0\rangle$, adopting the NRG philosophy that excitations on different energy scales are only weakly coupled.[22] Thus, the NRG generates a suitable low-energy Hamiltonian, allowing for the real-time dynamics of the problem to be explored on the exponentially long time scale $1/D_{\rm eff} \propto \Lambda^{M/2}$ using mainly the TD-DMRG.

B. Interfacing the NRG and DMRG

A key component of the hybrid-NRG is the interface between the TD-NRG and the complementary method of choice. This important aspect of the hybrid platform has been discussed in some detail in Ref. 22 from a general perspective. Below we provide essential details of the how the NRG and DMRG are interfaced.

Overall, there are five major steps in the hybrid NRG-DMRG algorithm. First, two NRG runs are performed up to (including) iteration M, one for the initial Hamiltonian $\mathcal{H}^i$ and another for the final Hamiltonian $\mathcal{H}^f$. During this step, which parallels the standard TD-NRG algorithm,[16,17] one records the NRG eigenenergies and transfer matrices at each iteration $m \leqslant M$, as well as the overlap matrices

$$\langle q_i; m|r; m\rangle = S_{q_i,r}(m). \tag{7}$$

These encode the overlap between the NRG eigenstates of the final Hamiltonian at iteration m (denoted by $|r; m\rangle$) and the NRG eigenstates of the initial Hamiltonian at the same iteration (denoted by $|s_i; m\rangle$). At the conclusion of this step one has produced, in particular, the effective low-energy Hamiltonian of Eq. (3) both for $\mathcal{H}^i$ and $\mathcal{H}^f$.

In the second step, one uses the DMRG[27] to compute the ground state of the low-energy Hamiltonian $\mathcal{H}^i_{M+1}$ corresponding to $\mathcal{H}^i$, which serves as our initial state $|\psi_0\rangle$. The state $|\psi_0\rangle$ so obtained has the form of a matrix product state,[13] where each chain site $M+n$ ($n = 1, \ldots, N-M$) in Eq. (3) is assigned a suitable matrix A^n. Viewing the N_s NRG eigenstates and eigenenergies kept at the conclusion of iteration M as forming the levels of a hyperimpurity, the latter is likewise assigned a matrix A^0, resulting in the matrix-product representation

$$|\psi_0\rangle \Longleftrightarrow A^0 A^1 A^2 \ldots A^{N-M}. \tag{8}$$

Given this form, the DMRG optimizes over the A matrices so as to minimize the energy of the targeted state with respect to $\mathcal{H}^i_{M+1}$.

Once at hand, the third step of the hybrid NRG-DMRG is to project the initial state $|\psi_0\rangle$ onto the low-energy subspace of the final Hamiltonian $\mathcal{H}^f$, in order to compute $|\chi_M\rangle = \hat{1}^+_M|\psi_0\rangle$. Generally speaking, if $|\psi_0\rangle$ has the formal expansion

$$|\psi_0\rangle = \sum_{q_i,e} c_{q_i,e}|q_i; M\rangle \otimes |e\rangle_{\text{chain}} \tag{9}$$

[here $|e\rangle_{\text{chain}}$ labels a basis state for the chain degrees of freedom in Eq. (3)], then a straightforward application of 1^+_M yields[22]

$$|\chi_M\rangle = \sum_{r,e} b_{r,e}|r; M\rangle \otimes |e\rangle_{\text{chain}} \tag{10}$$

with

$$b_{r,e} = \sum_{q_i} S^*_{q_i,r}(M) c_{q_i,e}. \tag{11}$$

This conversion rule is conveniently implemented in the DMRG, as it solely applies to the matrix A^0 that appears in the matrix-product representation of Eq. (8). Specifically, $A^0[s_i] \to \bar{A}^0[r]$ with

$$\bar{A}^0[r] = \sum_{q_i} S^*_{q_i,r}(M) A^0[q_i], \tag{12}$$

with all other matrices remaining unchanged.

The construction of $|\chi_M\rangle$ enables the fourth and fifth steps of the hybrid NRG-DMRG, which are (iv) propagation in time of

$$|\chi_M(t)\rangle = \hat{1}^+_M e^{-it\mathcal{H}^f}|\psi_0\rangle \approx e^{-it\mathcal{H}^f_{M+1}}|\chi_M\rangle \tag{13}$$

using the adaptive TD-DMRG[13] and the computation of $\langle\chi_M(t)|\hat{O}|\chi_M(t)\rangle$, and (v) the calculation of $\rho^{\text{red}}_{s,r}(M)$, which is then fed back into the TD-NRG to account for the contribution of the early NRG iterations with $m \leqslant M$. The latter computation implements the same backtracking algorithm of the TD-NRG.[16,17] Equation (13), we reiterate, is just the standard NRG approximation whereby the mixing of excitations at different iterations is neglected. Combined, steps four and five provide us with the two contributions to $O(t)$ in Eq. (2), i.e., that of the early iterations and that of the retained low-energy subspace.

III. RESULTS

A. Interacting resonant-level model

We shall demonstrate our hybrid NRG-DMRG approach by investigating quench dynamics in the IRLM, defined by the Hamiltonian

$$\mathcal{H} = \sum_k \epsilon_k c^\dagger_k c_k + E_d d^\dagger d + \frac{V}{\sqrt{N_k}}\sum_k \{c^\dagger_k d + \text{H.c.}\} + \frac{U}{N_k}\sum_{k,k'} :c^\dagger_k c_{k'}: \left(d^\dagger d - \frac{1}{2}\right). \tag{14}$$

Here, $d^\dagger$ creates an electron on the impurity level, $c^\dagger_k$ creates a band electron with momentum k, N_k denotes the number of distinct k points, and $:c^\dagger_k c_{k'}: = c^\dagger_k c_{k'} - \delta_{k,k'}\theta(-\epsilon_k)$ stands for normal ordering with respect to the filled Fermi sea. The basic energy scales in the problem include the level energy E_d and the hybridization width $\Gamma_0 = \pi\varrho V^2$, where ϱ is the conduction-electron density of states at the Fermi energy. The effect of the contact interaction is to renormalize the hybridization width at resonance according to $\Gamma_0 \to \Gamma_{\text{eff}} \approx D(\Gamma_0/D)^{1/(1+\alpha)}$, with $\alpha = 2\delta - \delta^2$ and $\delta = (2/\pi)\arctan(\pi\varrho U/2)$. Although the thermodynamics of the IRLM was investigated over 30 years ago,[24,25] there has been a recent surge of interest in its nonequilibrium properties, particularly for a biased two-lead setting.[7,8,10,28,29] Focusing on the single-band version of Eq. (14), we consider an abrupt shift of the level energy at time $t = 0$ from E^i_d to E^f_d, with the goal of tracking the time evolution of the level occupancy, $n_d(t) = \langle d^\dagger(t)d(t)\rangle$.

B. Hybrid chain

As discussed in Ref. 22, there are two sources of deviations from the continuum limit when considering quench dynamics on a pure Wilson chain: (i) internal reflections of currents caused by the exponentially decreasing hopping matrix

elements along the chain[30] (leading, in turn, to an exponential slowing down of the transport velocity); (ii) reflections at the end of the finite-size chain that propagate back to the impurity. While the former source of error is eliminated for an ordinary tight-binding chain, the latter point is unavoidable in nearly all practical calculations as the total chain length is limited by computational demands. Thus, one would like to simultaneously minimize the internal reflections and the transport velocity down the chain to accurately access long times.

Guided by these considerations, we propose to use a double Wilson chain, constructed by patching two separate Wilson chains (in contrast to the single Wilson chain employed in Ref. 22). The first M hopping matrix elements t_m with $0 \leqslant m \leqslant M-1$ are taken to be the customary Wilson hopping amplitudes[26] with the discretization parameter Λ_1. Further down the chain a second, smaller discretization parameter Λ_2 is used, with a magnitude close to but larger than one.[31,32] To reduce internal reflections, the transition from Λ_1 to Λ_2 is smoothed according to $t_{M+m} = \lambda_m^{-1/2} t_{M+m-1}$ with

$$\lambda_m = \begin{cases} \Lambda_1 - \frac{\Lambda_1 - \Lambda_2}{N_{\text{inter}}}(m+1), & 0 \leqslant m < N_{\text{inter}}, \\ \Lambda_2, & N_{\text{inter}} \leqslant m. \end{cases} \tag{15}$$

The merit of such a double Wilson chain is demonstrated in Fig. 1, where $n_d(t)$ is plotted following a quench from E_d^i to E_d^f. The interaction U is set to zero, to facilitate comparison with an exact continuum-limit solution in the wide-band limit,[17] as well as with an exact numerical solution on the hybrid chain, obtained by exact diagonalization of the single-particle eigenmodes. We set $\Gamma_0/D = 10^{-5}$, placing the basic time scale $1/\Gamma_0$ orders of magnitude beyond the reach of pure TD-DMRG. The parameter M was chosen such that $D\Lambda_1^{-M/2} \approx 20\Gamma_0$ is twice the maximal value of $|E_d|$ used.

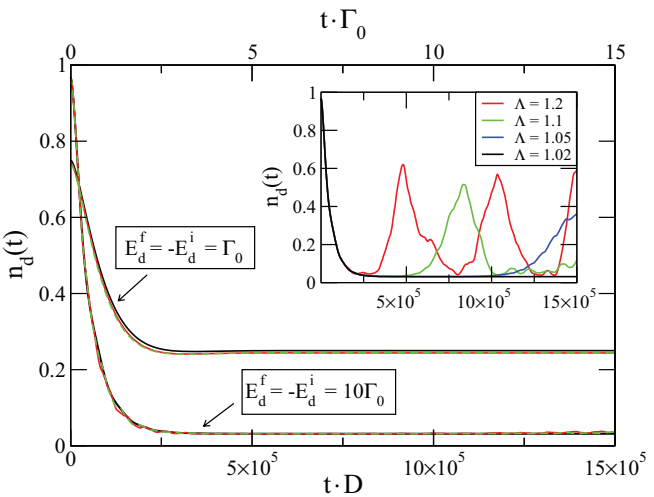

FIG. 1. (Color online) Time evolution of $n_d(t)$ on a double Wilson chain, following a sudden change of the level energy from E_d^i to E_d^f. Here $\Gamma_0/D = 10^{-5}$ and $U = 0$. The full red line depicts the exact solution on the double Wilson chain (obtained by exact diagonalization), the dashed green line displays the hybrid NRG-DMRG, and the full black line is the exact analytical continuum-limit solution (Ref. 17) in the wide-band limit. Chain parameters: $M = 29$, $\Lambda_1 = 1.8$, $\Lambda_2 = 1.02$, $N_{\text{inter}} = 4$, and $N = 180$. $N_s = 50$ states are retained both in the NRG and in the course of the TD-DMRG. Inset: Exact $n_d(t)$ on a pure Wilson chain, for $E_d^f = -E_d^i = 10\Gamma_0$ and different Λ's. Here $N = 500$ (1000) for $\Lambda \geqslant 1.1$ ($\Lambda \leqslant 1.05$).

Evidently, deviations between the continuum limit, the exact solution on the hybrid chain, and the hybrid NRG-DMRG approach are hardly discernible up to long time scales, well after the occupancy has relaxed to its new equilibrium value. For $E_d^f = -E_d^i = \Gamma_0$, the excellent agreement persists up to $t \gtrsim 30/\Gamma_0$, at which point all three curves begin to separate. For $E_d^f = -E_d^i = 10\Gamma_0$, the agreement extends up to slightly above $15/\Gamma_0$. As analyzed in the inset, an impractically small discretization parameter $\Lambda \approx \Lambda_2 = 1.02$ is needed to achieve a comparable representation of the continuum limit using a pure Wilson chain. Hence, by using a carefully designed double Wilson chain, one can work in effect with a discretization parameter $\Lambda \approx \Lambda_2$ extremely close to 1.

C. Interaction-enhanced oscillations

So far we have considered the case $U = 0$, for which exact results[17] are available. Next we address a finite contact interaction U and analyze its effect on $n_d(t)$. We note in passing that analytical corrections to the noninteracting limit were recently derived for weak coupling, $U/D \ll 1$, using the real-time renormalization group.[8] Here we focus primarily on stronger couplings, where qualitative differences from the noninteracting results are found.

As is well known, the IRLM is equivalent at low energies to its noninteracting counterpart, both describing a phase-shifted Fermi liquid. Near resonance, the effect of U in equilibrium is to renormalize Γ_0 to Γ_{eff}, hence one may expect $n_d(t)$ to follow the same curves as in Fig. 1 upon substituting $\Gamma_0 \to \Gamma_{\text{eff}}$. This, however, is not the case. In Fig. 2 we adjusted Γ_0 separately for each value of U so as to maintain a fixed

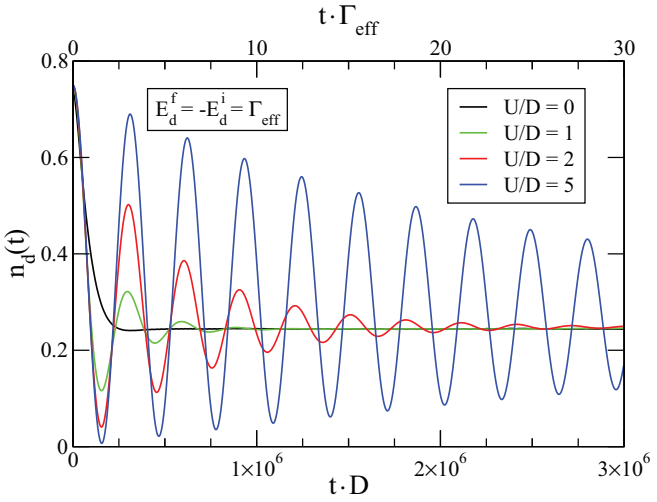

FIG. 2. (Color online) Same as Fig. 1, for $E_d^f = -E_d^i = \Gamma_{\text{eff}}$ and different values of U. Γ_0 was adjusted separately for each value of U so as to maintain $\Gamma_{\text{eff}}/D = 10^{-5}$. All other chain, NRG, and TD-DMRG parameters are the same as in Fig. 1.

$\Gamma_{\rm eff}/D = 10^{-5}$. To this end, we fixed $E_d/D = -10^{-5}$ and scanned Γ_0 using the hybrid NRG-DMRG until a ground-state occupancy of $n_d = 0.75$ was reached. As first reported in Ref. 22, interaction-enhanced oscillations gradually develop in $n_d(t)$ upon increasing U. For large $U/D > 1$, exemplified by $U/D = 5$, these oscillations decay on a time scale much longer than $1/\Gamma_{\rm eff}$, revealing the emergence of a new time scale unrelated to the thermodynamic ones. Note that, as for $U = 0$, our curves appear to faithfully represent the continuum limit up to $t \gtrsim 30/\Gamma_{\rm eff}$ for this moderate quench.

The extended time scales and supreme accuracy of the hybrid NRG-DMRG allow for a detailed quantitative analysis of the interaction-enhanced oscillations, which was previously impossible using the hybrid NRG-Chebyshev approach.[22] In particular, we can now address large values of $|E_d|/\Gamma_{\rm eff}$ that so far were inaccessible. The understanding of the interaction-enhanced oscillations employs a strong-coupling expansion in $1/U$, whose details are provided in the Appendix. Below we briefly discuss only the key points.

For $U \to \infty$, the impurity level and zeroth Wilson shell decouple from the rest of the chain, being confined to a combined valence of one. Within this subspace, the two eigenstates of the local Hamiltonian have the energies $\epsilon_\pm = (E_d/2) - U/4 \pm \sqrt{(E_d/2)^2 + V^2}$, hence $n_d(t)$ displays quantum beats with the frequency $\Omega = \epsilon_+ - \epsilon_- = 2\sqrt{(E_d/2)^2 + V^2}$.[22] For large but finite U, these coherent oscillations are damped by the residual coupling to the rest of the chain, which introduces a finite lifetime of the state ϵ_+. We expand to order $1/U$ about the $U \to \infty$ limit, which yields the residual coupling to the rest of the chain [see Eq. (A14)]. Using Fermi's golden rule, the decay time is found to be

$$\tau^{-1} = \pi \left(\frac{8D}{\pi^2 U}\right)^2 \frac{V^2}{\sqrt{(E_d/2)^2 + V^2}}. \tag{16}$$

Further neglecting rearrangements of the bath electrons (themselves being controlled by $1/U$), we deduce the functional form

$$n_d(t) = A[e^{-t/2\tau}\cos(\Omega t)\sqrt{1 - e^{-t/\tau}\cos^2\theta} - e^{-t/\tau}\sin\theta] + n_{\rm eq}(1 - e^{-t/\tau}) + n_d(0)e^{-t/\tau}, \tag{17}$$

where $n_{\rm eq}$ is the equilibrated long-time occupancy, while A and θ have no direct relation to any simple observable.

Panels (a) and (b) of Fig. 3 show typical fits of $n_d(t)$ to Eq. (17), using τ, Ω, A, θ, and $n_d(0) = 1 - n_{\rm eq}$ as fitting parameters. The fitting range, $t \cdot \Gamma_{\rm eff} \leqslant 10$, was carefully chosen to exclude any discretization error. Evidently, Eq. (17) describes the numerical curves quite well, further validating the expansion in $1/U$. The extracted values of Ω and τ, plotted in panels (c) and (d) for different quenches, practically coincide above $U/D \approx 10$ with the analytical predictions, confirming, in particular, that $\tau \propto U^2$. Hence, a new time scale with no thermodynamic counterpart is seen to emerge as U is increased.

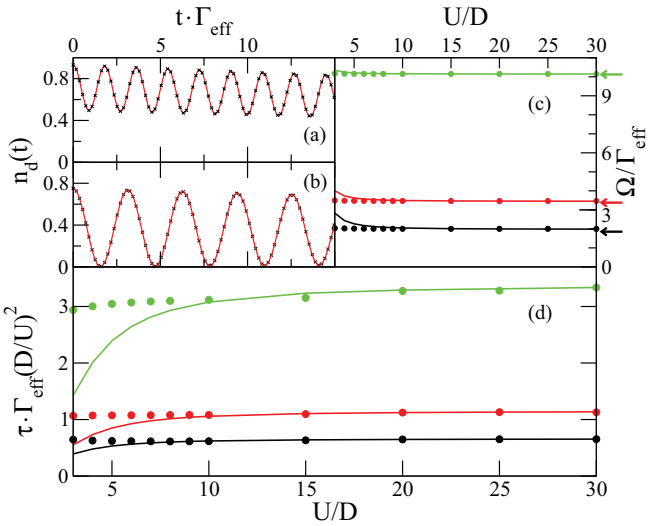

FIG. 3. (Color online) (a) Interaction-enhanced oscillations (red line) for $E_d^f = -E_d^i = 3\Gamma_{\rm eff}$ and $U/D = 10$, along with a fit to Eq. (17) (black crosses). (b) Same as (a), for $E_d^f = -E_d^i = \Gamma_{\rm eff}$. (c) The fitted frequency Ω vs U for $E_d^f/\Gamma_{\rm eff} = -E_d^i/\Gamma_{\rm eff} = 1$ (black circles), 3 (red circles), and 10 (green circles). Full lines display the analytical strong-coupling expression for Ω, employing the numerical values of V. Arrows on the right-hand side mark the asymptotic $U \to \infty$ values of Ω. (d) Same as (c) for the decay time τ. All remaining parameters are the same as in Fig. 2.

IV. SUMMARY

A new hybrid NRG-DMRG approach was devised that largely eliminates discretization errors hampering the TD-NRG, while boosting the TD-DMRG to time scales orders of magnitude beyond its natural reach. Two key ingredients lie at the heart of the approach. The first is the introduction of a new double Wilson chain that minimizes internal reflections along the chain while maximizing the round-trip time for a given chain length. This enabled access to continuum-limit results using a finite discretized chain, as demonstrated by comparison to the exact continuum-limit solution of the noninteracting resonant-level model. The other key component is usage of the NRG to construct an effective low-energy Hamiltonian that serves as input for TD-DMRG calculations on the optimized subchain. Since the effective bandwidth of the low-energy Hamiltonian can be orders of magnitude smaller than that of the original model, this allows access to time scales far beyond the reach of pure TD-DMRG.

With these improvements, the hybrid NRG-DMRG can address exceptionally long times with unparallel accuracy, as demonstrated by a detailed analysis of the interaction-enhanced oscillations in the IRLM. With increasing interaction strength, coherent oscillations gradually develop in $n_d(t)$, with a frequency that hardly depends on the interaction strength U and a decay time that grows asymptotically as U^2. Excellent agreement was obtained with analytical expressions derived using a strong-coupling expansion in $1/U$.

These outstanding capabilities of the hybrid NRG-DMRG open the door, so we hope, to accurate investigations of systems and coupling regimes that so far remained beyond reach. For example, the build-up of current in interacting quantum dots and single-molecule transistors in regimes where exponentially small energy scales are found. One particularly interesting direction are single-molecule devices showing

hysteretic I-V curves and negative differential conductances,[33] which may originate from conformational changes that take place in these complex molecules. Since the NRG is designed to take local interactions into account to all orders, our hybrid approach is neither limited to weak couplings nor to the high-temperature regime.

ACKNOWLEDGMENTS

This work was supported by the German-Israeli Foundation through Grant No. 1035-36.14, and by the Deutsche Forschungsgemeinschaft under AN 275/6-2 (F.G. and F.B.A).

APPENDIX: DETAILS OF THE STRONG-COUPLING EXPANSION

1. Derivation of effective Hamiltonian

In this Appendix, we provide details of the strong-coupling expansion about the $U \to \infty$ limit. Specifically, we carry out an expansion in $1/U$ to obtain the decay time τ of Eq. (16) and the functional form of the level occupancy specified in Eq. (17). Our starting point is the derivation of an effective Hamiltonian, valid to order $1/U$. To this end, we write the IRLM of Eq. (14) in the form

$$\mathcal{H} = \sum_{n=0}^{\infty} \xi_n \{f_{n+1}^\dagger f_n + f_n^\dagger f_{n+1}\} + \mathcal{H}_{\rm loc}, \tag{A1}$$

with the local Hamiltonian

$$\mathcal{H}_{\rm loc} = E_d d^\dagger d + V\{d^\dagger f_0 + f_0^\dagger d\} + U\left(f_0^\dagger f_0 - \tfrac{1}{2}\right)\left(d^\dagger d - \tfrac{1}{2}\right). \tag{A2}$$

Any particle-hole-symmetric band Hamiltonian can be cast in the form of Eq. (A1) using a Wilson-type tridigonalization procedure. Different band structures are distinguished by the hopping matrix elements ξ_n along the chain, the largest of which determines the bandwidth D. The conventional Wilson chain[26] is one example of such a tight-binding representation, where logarithmic discretization of the band is used as an approximation to obtain exponentially decreasing hopping matrix elements. We distinguish our general discussion from the more specific NRG-DMRG context by using a different notation (ξ_n as opposed to t_n) for the hopping matrix elements.

For large $U \gg D$, we begin by diagonalizing the local Hamiltonian $\mathcal{H}_{\rm loc}$, which is readily done by noting that $\mathcal{H}_{\rm loc}$ commutes with the combined number operator $\hat{N} = \hat{n}_d + \hat{n}_0$ with $\hat{n}_d = d^\dagger d$ and $\hat{n}_0 = f_0^\dagger f_0$. Introducing the state convention $|n_d,n_0\rangle$ where $n_d,n_0 \in \{0,1\}$ label the eigenvalues of $\hat{n}_d$ and $\hat{n}_0$, two obvious eigenstates of $\mathcal{H}_{\rm loc}$ are $|0,0\rangle$ and $|1,1\rangle$ with the eigenenergies $\epsilon_0 = U/4$ and $\epsilon_2 = U/4 + E_d$, respectively. The remaining two eigenstates in the $\hat{N} = 1$ sector are given by

$$|-\rangle = \alpha|1,0\rangle + \beta|0,1\rangle \quad \text{and} \quad |+\rangle = \beta|1,0\rangle - \alpha|0,1\rangle, \tag{A3}$$

with the corresponding energies

$$\epsilon_\mp = (E_d/2) - U/4 \mp \sqrt{(E_d/2)^2 + V^2}. \tag{A4}$$

Here, α and β are suitable real coefficients obeying $\alpha^2 + \beta^2 = 1$ and

$$\alpha\beta = -\frac{V}{2\sqrt{(E_d/2)^2 + V^2}} \tag{A5}$$

(only their product enters our calculation below).

At temperatures well below U, the two local states with $\hat{N} = 0,2$ become thermally inaccessible, leaving only the states $|\pm\rangle$ of the $\hat{N} = 1$ sector thermally active. Coupling to the rest of the chain, specifically the term $\xi_0(f_1^\dagger f_0 + f_0^\dagger f_1)$, introduces, however, virtual transitions to the excited states, which we account for by resorting to a Schrieffer-Wolff–type transformation.[34] Specifically, we seek a canonical transformation

$$\mathcal{H}_{\rm S} = e^S \mathcal{H} e^{-S} \tag{A6}$$

with a suitable anti-Hermitian operator S such that the low-energy subspace with $\hat{N} = 1$ is decoupled to order ξ_0^2 from the high-energy subspace with $\hat{N} = 0,2$.[35] To this end, we introduce two complementary projection operators, P and $Q = 1 - P$, where $P = (2 - \hat{N})\hat{N}$ projects onto the $\hat{N} = 1$ sector. The Hamiltonian $\mathcal{H}$ is then divided into an "unperturbed" part $\mathcal{H}_0$ and a "perturbation" $\mathcal{H}_1$, where

$$\mathcal{H}_0 = P\mathcal{H}P + Q\mathcal{H}Q = \mathcal{H}_{\rm loc} + \sum_{n=1}^{\infty} \xi_n \{f_{n+1}^\dagger f_n + f_n^\dagger f_{n+1}\} \tag{A7}$$

and

$$\mathcal{H}_1 = P\mathcal{H}Q + Q\mathcal{H}P = \xi_0(f_1^\dagger f_0 + f_0^\dagger f_1). \tag{A8}$$

Using the formal expansion

$$\mathcal{H}_{\rm S} = \mathcal{H}_0 + \mathcal{H}_1 + [S,\mathcal{H}_0] + [S,\mathcal{H}_1] + \tfrac{1}{2}[S,[S,\mathcal{H}_0]] + \cdots \tag{A9}$$

and exploiting the fact that S is proportional to ξ_0 at leading order, one can group the different terms in Eq. (A9) according to powers in ξ_0. The requirement that no coupling is left to order ξ_0^2 between the high- and low-energy subspaces is satisfied by requiring that

$$\mathcal{H}_1 + [S,\mathcal{H}_0] = \mathcal{O}\left(\xi_0^3\right), \tag{A10}$$

resulting in

$$\mathcal{H}_{\rm S} = \mathcal{H}_0 + \tfrac{1}{2}[S,\mathcal{H}_1] + \mathcal{O}\left(\xi_0^3\right). \tag{A11}$$

Equation (A10) has the formal solution

$$S = -\frac{1}{\mathcal{L}_0}\mathcal{H}_1 + \mathcal{O}\left(\xi_0^3\right), \tag{A12}$$

where $\mathcal{L}_0$ is the Liouville operator defined by $\mathcal{L}_0\hat{O} = [\hat{O},\mathcal{H}_0]$. To leading order in $1/U$ one can substitute $\mathcal{L}_0 \to \mathcal{L}_{\rm loc}$ with $\mathcal{L}_{\rm loc}\hat{O} = [\hat{O},\mathcal{H}_{\rm loc}]$ in Eq. (A12), corresponding to setting $\mathcal{H}_0 \to \mathcal{H}_{\rm loc}$. This approximation for S yields the explicit expression $S = \tilde{S} - \tilde{S}^\dagger$ with

$$\tilde{S} = \left[\frac{\beta\xi_0}{\epsilon_2 - \epsilon_-}|1,1\rangle\langle -| - \frac{\alpha\xi_0}{\epsilon_2 - \epsilon_+}|1,1\rangle\langle +| - \frac{\alpha\xi_0}{\epsilon_0 - \epsilon_-}|-\rangle\langle 0,0| + \frac{\beta\xi_0}{\epsilon_0 - \epsilon_+}|+\rangle\langle 0,0|\right] f_1, \tag{A13}$$

which follows from a suitable decomposition of $f_0^\dagger$ into Hubbard eigenoperators of $\mathcal{L}_{\rm loc}$. Since $U \gg |E_d|, V$, one can further replace each of the energy denominators in Eq. (A13) with $U/2$. Substituting the resulting expression for S into Eq. (A11) and projecting $\mathcal{H}_{\rm S}$ onto the low-energy subspace, one finally arrives at the following effective low-energy Hamiltonian, valid to order $1/U$:

$$\mathcal{H}_{\rm eff} = \sum_{n=1}^{\infty} \xi_n \{ f_{n+1}^\dagger f_n + f_n^\dagger f_{n+1} \} + \sum_{p=\pm} \epsilon_p |p\rangle\langle p| + \frac{2\xi_0^2}{U}(\beta^2 - \alpha^2)\,[|-\rangle\langle -| - |+\rangle\langle +|] : f_1^\dagger f_1 : - \frac{4\xi_0^2}{U}\alpha\beta\,[|-\rangle\langle +| + |+\rangle\langle -|] : f_1^\dagger f_1 : . \tag{A14}$$

Here, $: f_1^\dagger f_1 : = f_1^\dagger f_1 - 1/2$ represents normal ordering with respect to the filled Fermi sea of the truncated chain.

2. Decay time τ

The effective Hamiltonian of Eq. (A14) contains two interaction terms, one representing static potential scattering with an overall sign that depends on the "impurity" configuration $|\pm\rangle$, and another involving transitions between the states $|-\rangle$ and $|+\rangle$. It is this latter term that is responsible for the decay time τ. For $U \to \infty$, when no transitions are allowed between the two "impurity" states, local observables display quantum beats with the frequency $\Omega = \epsilon_+ - \epsilon_- = 2\sqrt{(E_d/2)^2 + V^2}$.[22] Once U is made finite, the system can relax from the locally excited state $|+\rangle$ to $|-\rangle$, which damps the quantum beats. The associated decay time τ can be estimated for large U using Fermi's golden rule. The basic relaxation mechanism involves the transition from $|+\rangle$ to $|-\rangle$ while creating a particle-hole excitation in the Fermi sea of the truncated chain. Denoting the local density of states corresponding to $f_1^\dagger$ in the truncated chain by $\tilde{\varrho}$, a straightforward calculations yields

$$\tau^{-1} = 2\pi \left(\frac{4\alpha\beta}{U} \xi_0^2 \right)^2 \tilde{\varrho}^2 \Omega, \tag{A15}$$

where $\tilde{\varrho}^2$ represents the combined density of states for particle-hole excitations and Ω is the available window of energy for such excitations.

Equation (A15) involves the combination $\xi_0^2 \tilde{\varrho}$, which may appear at first sight as an unknown quantity that depends on details of the band structure. Remarkably, for a particle-hole symmetric band of the type considered here one has the identity

$$\xi_0^2 \tilde{\varrho} = \frac{1}{\pi^2 \varrho}, \tag{A16}$$

which follows from the locator expansion $g(z) = [z - \xi_0^2 \tilde{g}(z)]^{-1}$, relating the Green function g of site $j = 0$ with respect to the free chain Hamiltonian of Eq. (A1) and the Green function $\tilde{g}$ of site $j = 1$ with respect to the truncated chain Hamiltonian of Eq. (A14). Particle-hole symmetry implies that $g(0 + i\eta)$ and $\tilde{g}(0 + i\eta)$ are purely imaginary and equal to $-i\pi\varrho$ and $-i\pi\tilde{\varrho}$, respectively, hence $-i\pi\varrho = -i/(\xi_0^2 \pi \tilde{\varrho})$. Inserting Eqs. (A5) and (A16) into Eq. (A15) and setting $\varrho = 1/(2D)$, one finally obtains the decay time of Eq. (16).

3. Functional form of $n_d(t)$

To compute $n_d(t)$, we begin by writing the time-dependent state of the system in the form

$$|\psi(t)\rangle = c_-(t) e^{-i\epsilon_- t} |-\rangle \otimes |\psi_{\rm bath}^{(-)}(t)\rangle + c_+(t) e^{-i\epsilon_+ t} |+\rangle \otimes |\psi_{\rm bath}^{(+)}(t)\rangle, \tag{A17}$$

where $|\psi_{\rm bath}^{(\pm)}(t)\rangle$ pertain to the chain degrees of freedom [i.e., $f_1^\dagger, f_2^\dagger, \ldots$ in Eq. (A14)]. Our convention for the coefficients $c_\pm(t)$ is that they are real and positive, with all residual time dependence contained in $|\psi_{\rm bath}^{(\pm)}(t)\rangle$. The latter states are taken to be normalized to unity, i.e., $\langle \psi_{\rm bath}^{(\pm)}(t) | \psi_{\rm bath}^{(\pm)}(t) \rangle = 1$, such that $n_\pm(t) = c_\pm^2(t)$ [$n_\pm(t)$ being the time-dependent occupancy of the "impurity" state $|\pm\rangle$]. In terms of the coefficients $c_\pm(t)$, occupancy of the d level takes the form

$$n_d(t) = \alpha^2 c_-^2(t) + \beta^2 c_+^2(t) + 2\alpha\beta c_-(t) c_+(t) \times {\rm Re}\{ e^{-i\Omega t} \langle \psi_{\rm bath}^{(-)}(t) | \psi_{\rm bath}^{(+)}(t) \rangle \}, \tag{A18}$$

where we have made use of the explicit forms of the states $|\pm\rangle$ detailed in Eq. (A3).

As shown in the previous subsection, $n_+(t)$ decays to zero at the golden rule level with the decay time τ, implying that

$$c_+(t) = \sqrt{n_+(t)} = c_+(0) e^{-t/(2\tau)}, \tag{A19}$$

$$c_-(t) = \sqrt{1 - n_+(t)} = \sqrt{1 - n_+(0) e^{-t/\tau}}. \tag{A20}$$

Thus, $n_d(t)$ relaxes at long times to $n_{\rm eq} = \alpha^2$. The opposite limit of short time is obtained by setting $t \to 0$ in Eq. (A18), which yields

$$n_d(0) = \alpha^2 c_-^2(0) + \beta^2 c_+^2(0) + 2\alpha\beta c_-(0) c_+(0) {\rm Re}\{ \langle \psi_{\rm bath}^{(-)}(0) | \psi_{\rm bath}^{(+)}(0) \rangle \}. \tag{A21}$$

These observations allow us to rewrite Eq. (A18) in the form

$$n_d(t) = n_{\rm eq}(1 - e^{-t/\tau}) + n_d(0) e^{-t/\tau} + 2\alpha\beta c_-(t) c_+(t) {\rm Re}\{ e^{-i\Omega t} \langle \psi_{\rm bath}^{(-)}(t) | \psi_{\rm bath}^{(+)}(t) \rangle \} - 2\alpha\beta c_-(0) c_+(0) {\rm Re}\{ \langle \psi_{\rm bath}^{(-)}(0) | \psi_{\rm bath}^{(+)}(0) \rangle \} e^{-t/\tau}. \tag{A22}$$

To make further progress, we neglect the time dependence of the overlap $\langle \psi_{\rm bath}^{(-)}(t) | \psi_{\rm bath}^{(+)}(t) \rangle$, omitting thereby rearrangements of the bath electrons. Indeed, since the latter processes are controlled by weak impurity scattering of magnitude $1/U$, one may expect the overlap to display a weak power-law decay in time with an exponent that vanishes as $1/U$ for $U \to \infty$. Further noting that $\langle \psi_{\rm bath}^{(-)}(0) | \psi_{\rm bath}^{(+)}(0) \rangle$ is purely real [a result that follows from the fact that $|\psi(0)\rangle$ is the ground state of a Hamiltonian with purely real matrix elements], one can approximate the last two lines in Eq. (A22) by

$$2\alpha\beta \langle \psi_{\rm bath}^{(-)}(0) | \psi_{\rm bath}^{(+)}(0) \rangle \times [c_-(t) c_+(t) \cos(\Omega t) - c_-(0) c_+(0) e^{-t/\tau}]. \tag{A23}$$

Finally, inserting Eqs. (A19) and (A20) into Eq. (A23), one recovers Eq. (17) with $c_-(0) = \sin\theta$ and $A = 2\alpha\beta c_+(0) \langle \psi_{\rm bath}^{(-)}(0) | \psi_{\rm bath}^{(+)}(0) \rangle$.

Let us reiterate the three approximations which entered the derivation of $n_d(t)$: (i) restriction of the full Hilbert

space to the low-energy subspace with $\hat{N} = 1$; (ii) Fermi's golden rule approximation for $n_+(t)$; (iii) neglect of the time dependence of $\langle \psi^{(-)}_{\rm bath}(t)|\psi^{(+)}_{\rm bath}(t)\rangle$. Being controlled by $1/U$, all three approximations are expected to improve in accuracy upon increasing U, as supported by our NRG calculations.

[1] L. Perfetti, P. A. Loukakos, M. Lisowski, U. Bovensiepen, H. Berger, S. Biermann, P. S. Cornaglia, A. Georges, and M. Wolf, Phys. Rev. Lett. **97**, 067402 (2006).

[2] F. Schmitt, P. S. Kirchmann, U. Bovensiepen, R. G. Moore, L. Rettig, M. Krenz, J.-H. Chu, N. Ru, L. Perfetti, D. H. Lu, M. Wolf, I. R. Fisher, and Z.-X. Shen, Science **321**, 1649 (2008).

[3] M. Greiner, O. Mandel, T. W. Hänsch, and I. Bloch, Nature (London) **419**, 51 (2002); T. Kinoshita, T. Wenger, and D. S. Weiss, *ibid.* **440**, 900 (2006).

[4] S. Trotzky, Y.-A. Chen, A. Flesch, I. P. McCulloch, U. Schollwöck, J. Eisert, and I. Bloch, Nat. Phys. **8**, 325 (2012).

[5] J. M. Elzerman, R. Hanson, L. H. W. van Beveren, B. Witkamp, L. M. K. Vandersypen, and L. P. Kouwenhoven, Nature (London) **430**, 431 (2004).

[6] J. R. Petta, A. C. Johnson, J. M. Taylor, E. A. Laird, A. Yacoby, M. D. Lukin, C. M. Marcus, M. P. Hanson, and A. C. Gossard, Science **309**, 2180 (2005).

[7] M. Pletyukhov, D. Schuricht, and H. Schoeller, Phys. Rev. Lett. **104**, 106801 (2010); S. Andergassen, M. Pletyukhov, D. Schuricht, H. Schoeller, and L. Borda, Phys. Rev. B **83**, 205103 (2011); C. Karrasch, S. Andergassen, M. Pletyukhov, D. Schuricht, L. Borda, V. Meden, and H. Schoeller, Europhys. Lett. **90**, 30003 (2010).

[8] D. M. Kennes, O. Kashuba, M. Pletyukhov, H. Schoeller, and V. Meden, Phys. Rev. Lett. (to be published), arXiv:1211.0293.

[9] A. Hackl and S. Kehrein, J. Phys.: Condens. Matter **21**, 015601 (2009); A. Hackl, M. Vojta, and S. Kehrein, Phys. Rev. B **80**, 195117 (2009); P. Wang and S. Kehrein, *ibid.* **82**, 125124 (2010).

[10] D. M. Kennes, S. G. Jakobs, C. Karrasch, and V. Meden, Phys. Rev. B **85**, 085113 (2012); D. M. Kennes and V. Meden, Phys. Rev. B (to be published), arXiv:1210.1340.

[11] M. Pletyukhov and H. Schoeller, Phys. Rev. Lett. **108**, 260601 (2012).

[12] G. Vidal, Phys. Rev. Lett. **93**, 040502 (2004); A. J. Daley, C. Kollath, U. Schollwöck, and G. Vidal, J. Stat. Mech.: Theor. Exp. (2004) P04005; S. R. White and A. E. Feiguin, Phys. Rev. Lett. **93**, 076401 (2004).

[13] For a recent review on the DMRG and TD-DMRG, see U. Schollwöck, Ann. Phys. **326**, 96 (2011).

[14] P. Schmitteckert, Phys. Rev. B **70**, 121302 (2004); A. Branschädel, G. Schneider, and P. Schmitteckert, Ann. Phys. **522**, 657 (2010).

[15] K. A. Al-Hassanieh, A. E. Feiguin, J. A. Riera, C. A. Büsser, and E. Dagotto, Phys. Rev. B **73**, 195304 (2006); L. G. G. V. Dias da Silva, F. Heidrich-Meisner, A. E. Feiguin, C. A. Büsser, G. B. Martins, E. V. Anda, and E. Dagotto, *ibid.* **78**, 195317 (2008); F. Heidrich-Meisner, A. E. Feiguin, and E. Dagotto, *ibid.* **79**, 235336 (2009).

[16] F. B. Anders and A. Schiller, Phys. Rev. Lett. **95**, 196801 (2005).

[17] F. B. Anders and A. Schiller, Phys. Rev. B **74**, 245113 (2006).

[18] S. Weiss, J. Eckel, M. Thorwart, and R. Egger, Phys. Rev. B **77**, 195316 (2008).

[19] L. Mühlbacher and E. Rabani, Phys. Rev. Lett. **100**, 176403 (2008).

[20] P. Werner, T. Oka, and A. J. Millis, Phys. Rev. B **79**, 035320 (2009); P. Werner, T. Oka, M. Eckstein, and A. J. Millis, *ibid.* **81**, 035108 (2010).

[21] M. Schiró and M. Fabrizio, Phys. Rev. B **79**, 153302 (2009).

[22] E. Eidelstein, A. Schiller, F. Güttge, and F. B. Anders, Phys. Rev. B **85**, 075118 (2012).

[23] H. Tal Ezer and R. Kosloff, J. Chem. Phys. **81**, 3967 (1984).

[24] P. B. Vigman and A. M. Finkelstein, Zh. Eksp. Theor. Fiz. **75**, 204 (1978) [Sov. Phys. JETP **48**, 102 (1978)].

[25] P. Schlottmann, Phys. Rev. B **22**, 622 (1980).

[26] K. G. Wilson, Rev. Mod. Phys. **47**, 773 (1975); R. Bulla, T. A. Costi, and T. Pruschke, *ibid.* **80**, 395 (2008).

[27] S. R. White, Phys. Rev. Lett. **69**, 2863 (1992); Phys. Rev. B **48**, 10345 (1993).

[28] P. Mehta and N. Andrei, Phys. Rev. Lett. **96**, 216802 (2006).

[29] E. Boulat, H. Saleur, and P. Schmitteckert, Phys. Rev. Lett. **101**, 140601 (2008).

[30] P. Schmitteckert, J. Phys.: Conf. Ser. **220**, 012022 (2010).

[31] A. Weichselbaum, F. Verstraete, U. Schollwöck, J. I. Cirac, and Jan von Delft, Phys. Rev. B **80**, 165117 (2009).

[32] Another motivation for using a modified Wilson chain was recently given in Ref. 31. These authors adopted a different point of view and a different construction based upon Wilson's original discretization of the bath.

[33] For a review see, e.g., M. Galperin, M. A. Ratner, and A. Nitzan, J. Phys.: Condens. Matter **19**, 103201 (2007).

[34] J. R. Schrieffer and P. A. Wolff, Phys. Rev. **149**, 491 (1966).

[35] Although $\xi_0 \sim D$ is not a small energy scale by itself, the expansion parameter governing the Schrieffer-Wolff–type transformation is ξ_0/U, which is assumed to be small.